Supplementary Figures and Legends

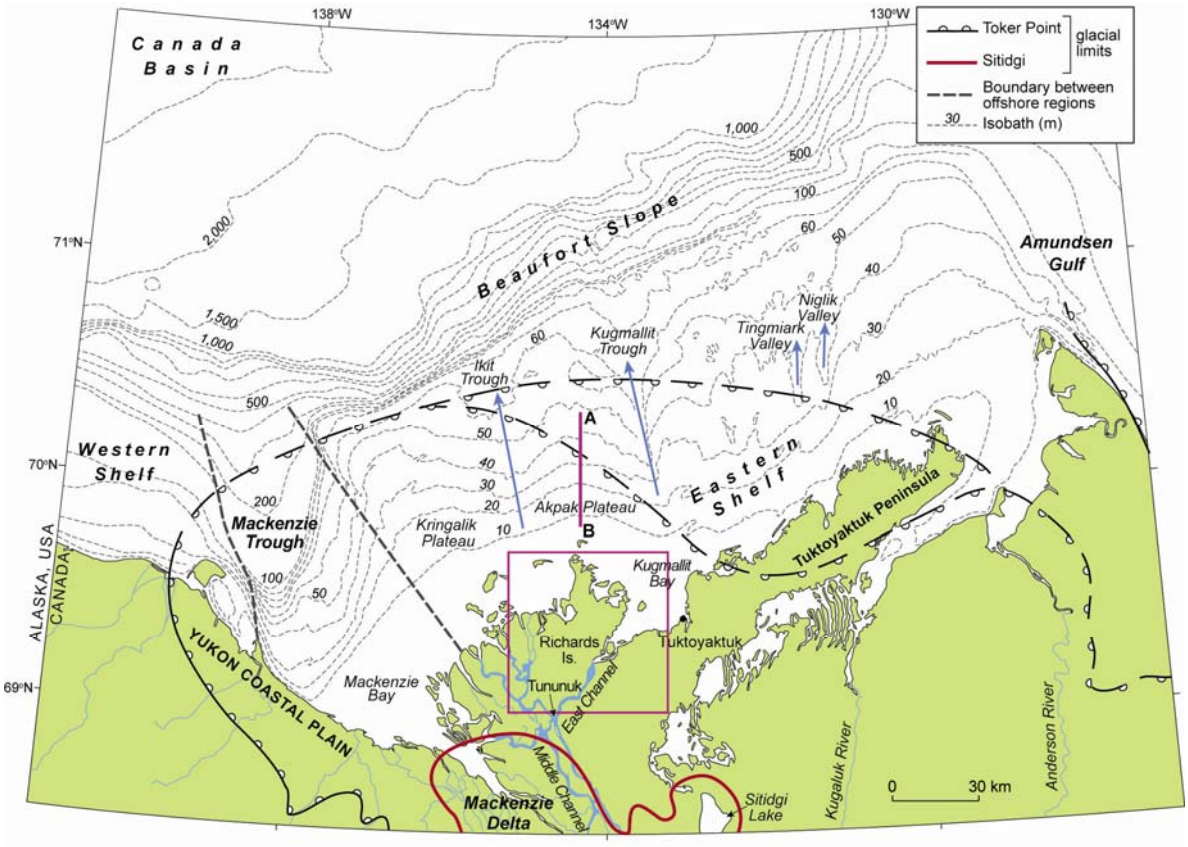

Supplementary Figure 1. Canadian Arctic Coastal Plain and bathymetry of the Beaufort Continental Shelf. A system of submerged valleys (Ikit, Kugmallit, Tingmiark and Niglik) crosses the shelf[8], separating plateaus and plains (e.g. Kringalik and Akpak plateaus). Two glacial limits are marked for the Toker Point Stade in the Tuktoyaktuk Peninsula region, reflecting uncertainty about the topographic profile of the ice sheet in this area[30]. Line A to B marks location of seismostratigraphic section shown in Supplementary Fig. 2. Purple rectangle marks location of Fig. 2.

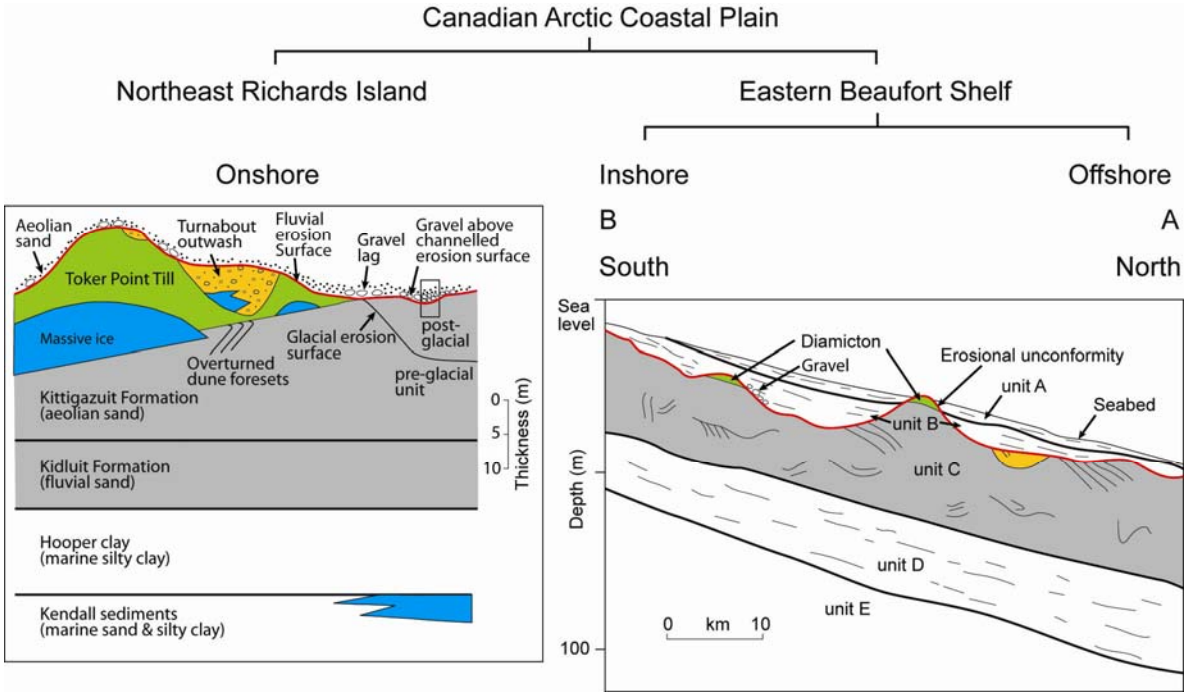

Supplementary Figure 2. Onshore-offshore correlation of (1) the Kittigazuit Formation and Kidluit Formation with unit C, modified from ref. 31 (grey), (2) Toker Point till with diamicton[31] (green), (3) erosion surface (red line), and (4) glaciofluvial outwash of the Turnabout Member with infilled depressions (yellow). Onshore lithostratigraphy of northern Richards Island is modified from ref. 32. Offshore seismostratigraphy shows the upper 100 m of sediments beneath the seafloor of the eastern Beaufort Shelf, modified from ref. 7, with gravel indicated above the erosional unconformity (see ref. 33). Location shown in Supplementary Fig. 1 between 'A' and 'B'. Rectangle indicates stratigraphic position of Supplementary Fig. 3.

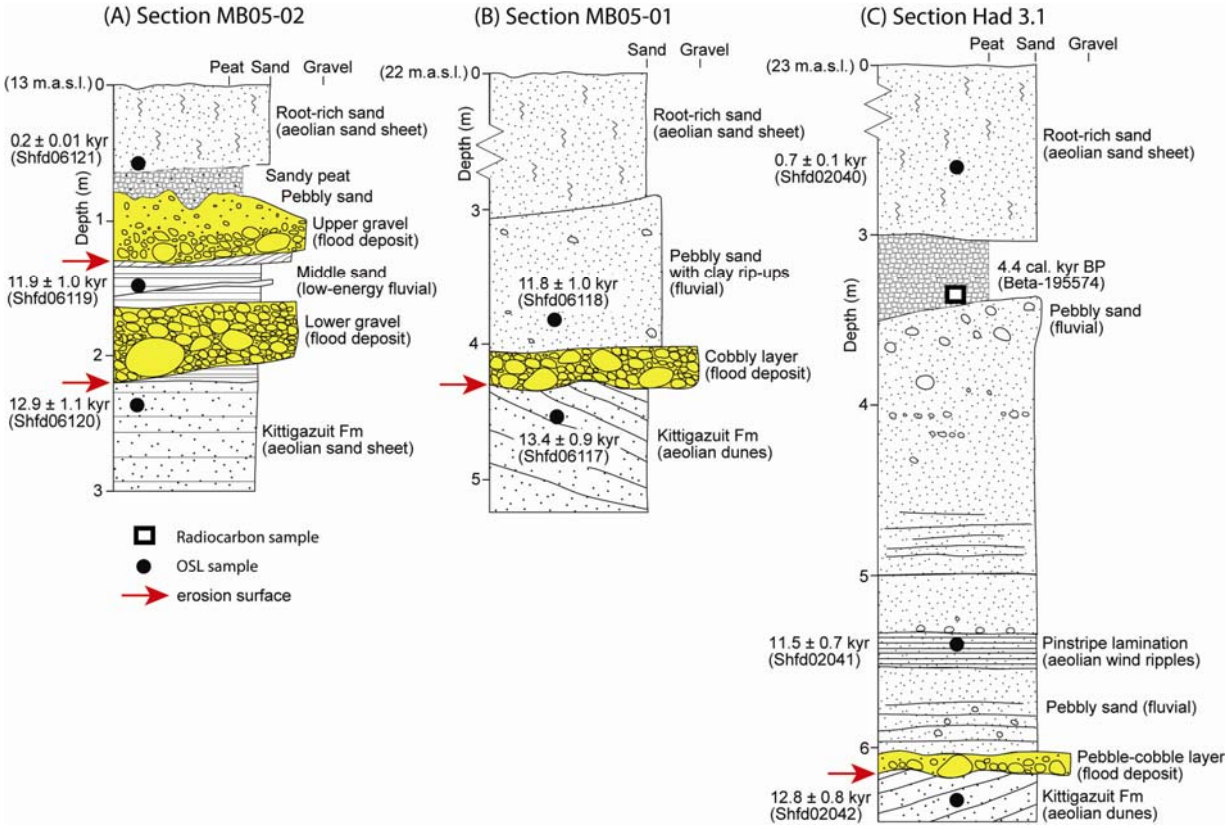

Supplementary Figure 3. (A)–(C) Onshore stratigraphic sections through fluvial gravels (yellow) and erosion surfaces reported in this study. Pairs of optical dates with their 1 sigma uncertainties are marked above and below the lower gravel. Location of sections shown on Fig. 2.

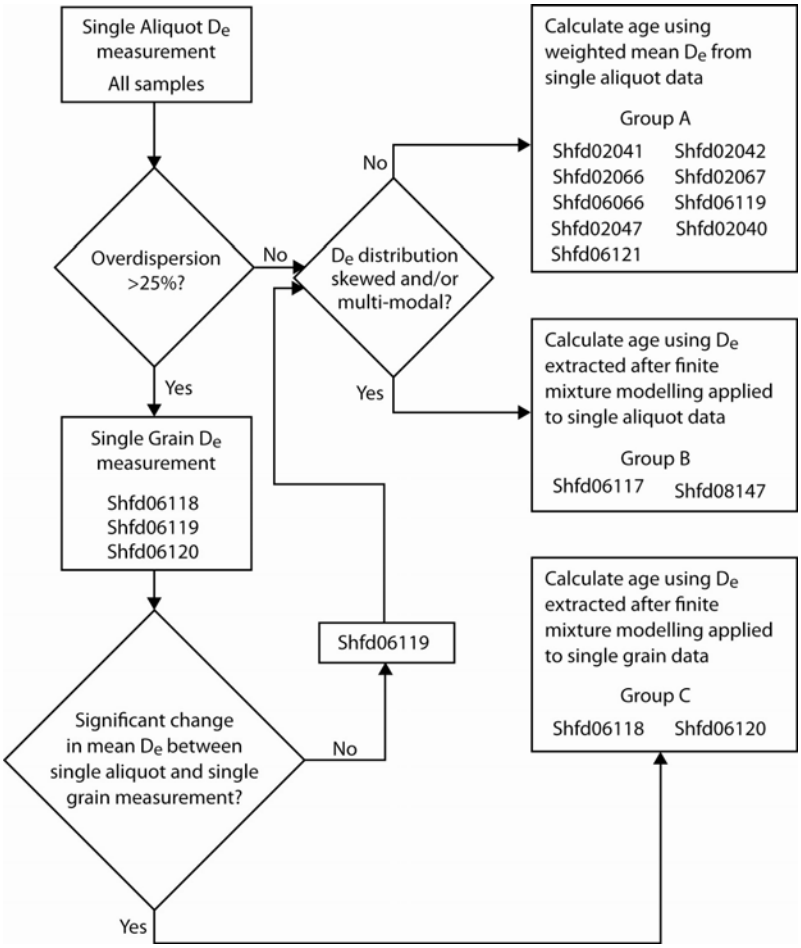

Supplementary Figure 4. Flow diagram of OSL decision-making process used to determine whether further measurement at the single grain level was undertaken and the type of statistical analysis carried out on D_e values from the samples.

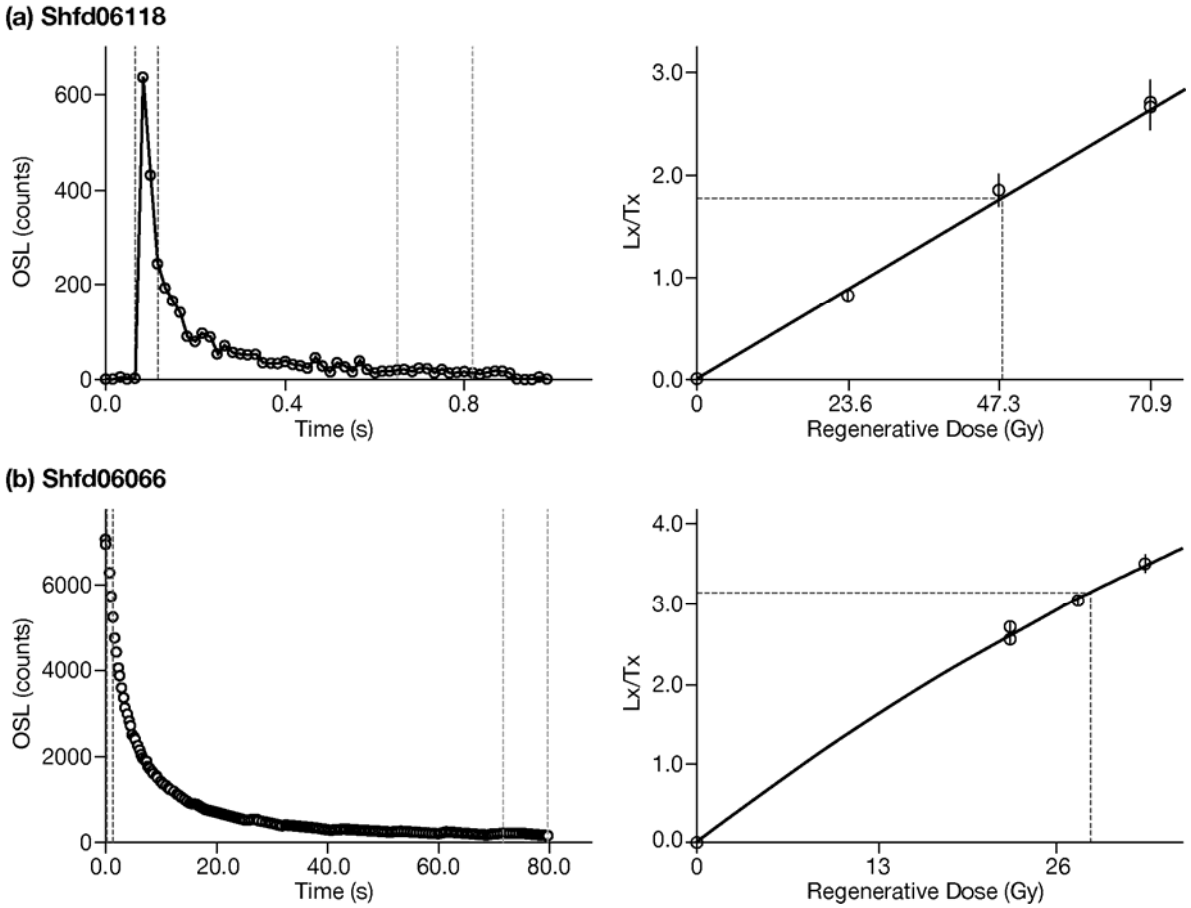

Supplementary Figure 5. Examples of OSL shine down curves and SAR growth curves for OSL samples presented in Table 1; (a) single grain measurements; (b) 9.6 mm diameter single aliquot measurements which comprised approximately 8000 grains per aliquot for samples from sites CP3.11 and Had3.1, 4000 grains for sites MB05 and SB05, and 1500 grains from site SB08. Dashed lines in left-hand plots denote integrals used for signal and background in SAR growth curve. Vertical bars associated with points on right-hand plots indicate counting statistics, instrumental errors and sensitivity correction errors.

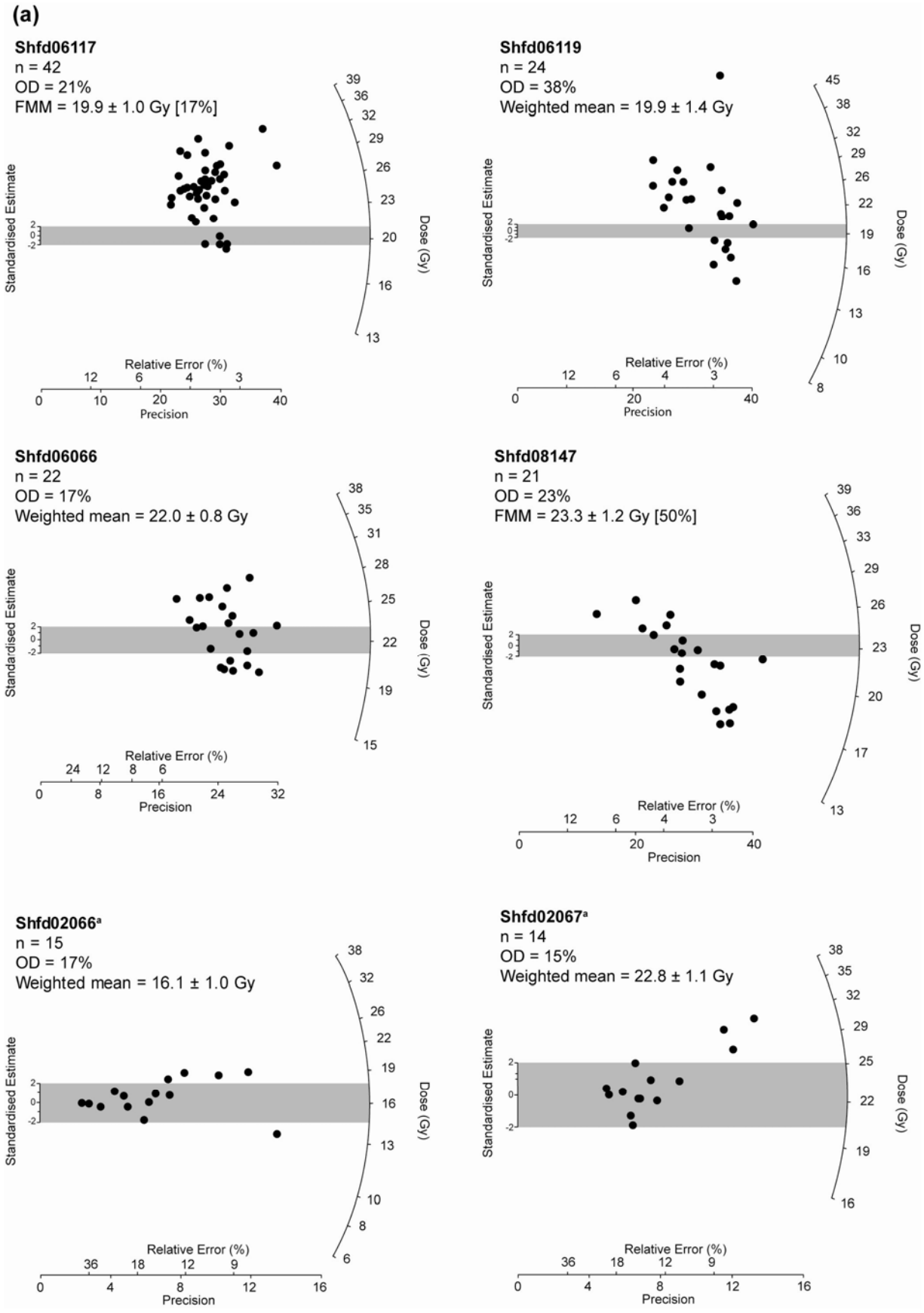
(a)
Shfd06117
n = 42
OD = 21%
FMM = 19.9 ± 1.0 Gy [17%]
Shfd06119
n = 24
OD = 38%
Weighted mean = 19.9 ± 1.4 Gy
Shfd06066
n = 22
OD = 17%
Weighted mean = 22.0 ± 0.8 Gy
Shfd08147
n = 21
OD = 23%
FMM = 23.3 ± 1.2 Gy [50%]
Shfd02066[a]
n = 15
OD = 17%
Weighted mean = 16.1 ± 1.0 Gy
Shfd02067[a]
n = 14
OD = 15%
Weighted mean = 22.8 ± 1.1 Gy
Standardised Estimate
Dose (Gy)
Relative Error (%)
Precision

(a) continued

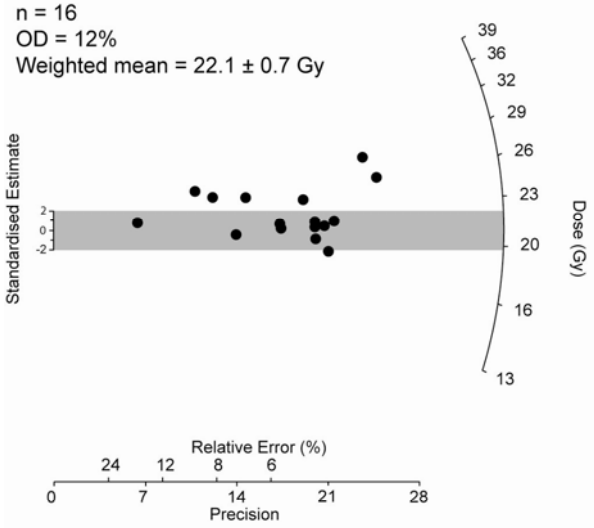
Shfd02041[a]
n = 16
OD = 12%
Weighted mean = 22.1 ± 0.7 Gy
Standardised Estimate
Dose (Gy)
Relative Error (%)
Precision

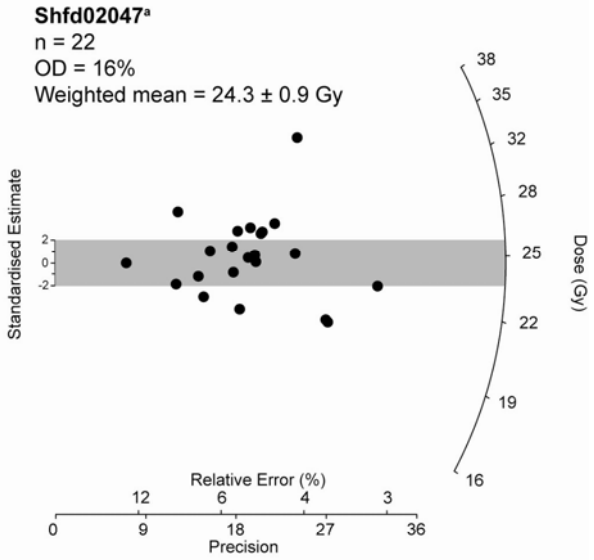
Shfd02047[a]
n = 22
OD = 16%
Weighted mean = 24.3 ± 0.9 Gy
Standardised Estimate
Dose (Gy)
Relative Error (%)
Precision

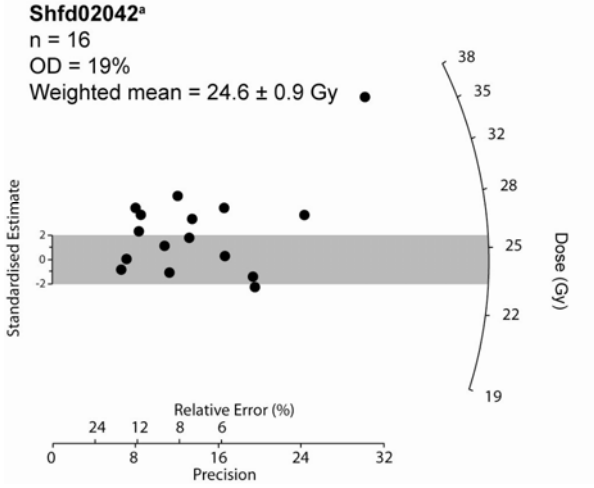
Shfd02042[a]
n = 16
OD = 19%
Weighted mean = 24.6 ± 0.9 Gy
Standardised Estimate
Dose (Gy)
Relative Error (%)
Precision

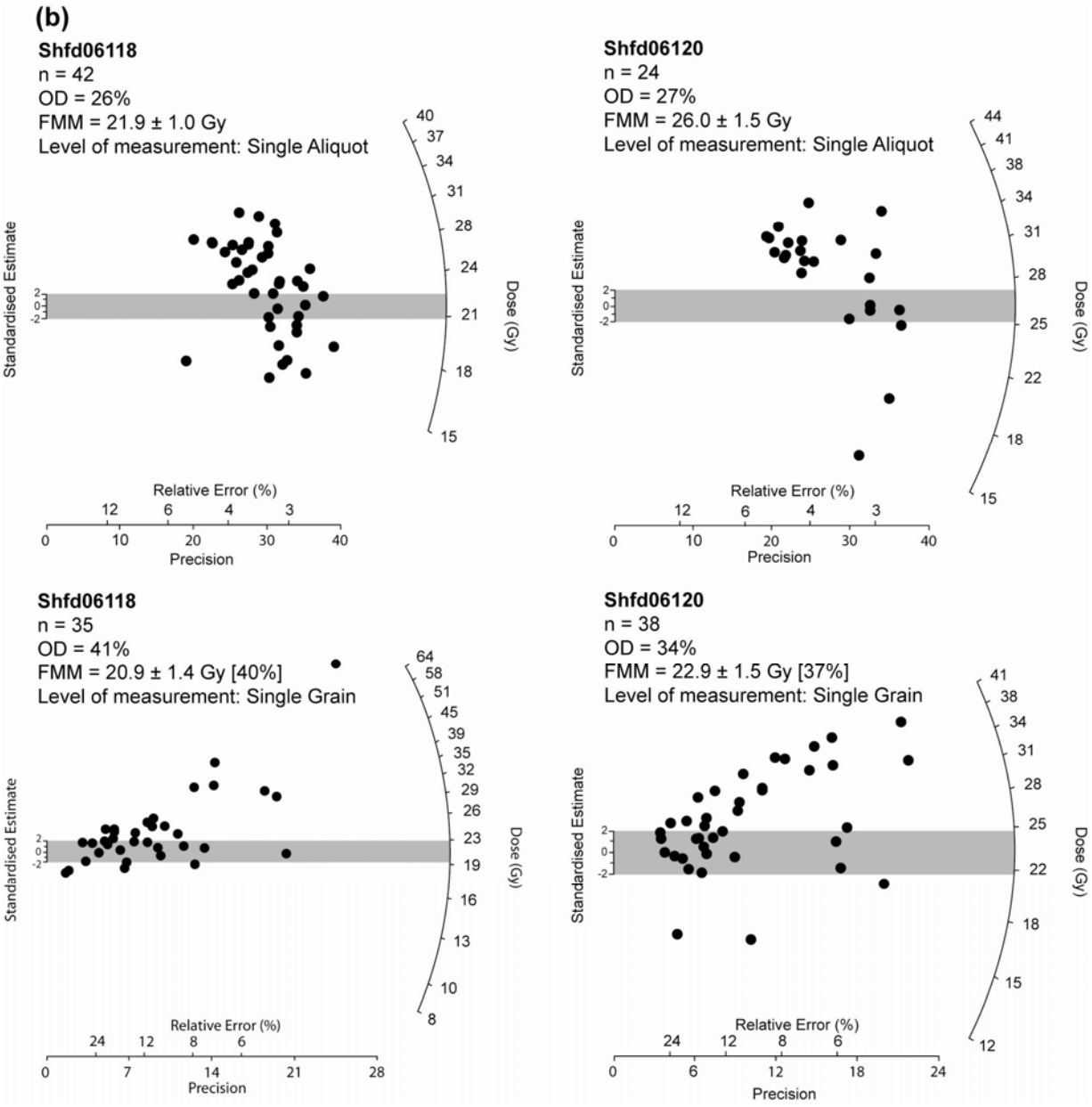

Supplementary Figure 6. Radial plots of D_e data for each sample with uncertainties incorporating an instrumental uncertainty (1.5% single aliquot; 2.5% single grain), beta source calibration, counting statistics and growth curve fitting. (a) Samples measured at the single aliquot level; (b) samples measured at the single aliquot level which required further measurement at the single grain level to derive age estimates. Greyed area indicates 2 standardised estimates around the central D_e value. Also shown are number of grains/aliquots measured, the over dispersion (OD) values and the final D_e with associated standard error used for age calculation purposes. Where Finite Mixture modeling (FMM) was employed, the proportion of data represented by this component is given in brackets after the D_e value. [a] D_e data for samples reported in Ref. 6.

Supplementary Methods

Optical Dating

All samples were collected from freshly exposed sedimentary sections using opaque PVC tubing which was immediately sealed with opaque endcaps and tape. Samples were prepared under low-intensity red lighting by removing carbonates and organic material with HCl and H_2O_2 and dry sieving to isolate sand in the range 90−250 μm. Quartz was separated from heavy minerals with a density separation using sodium polytungstate (S.G. 2.7 g cm^{-3}) and a 45 min 40% HF etch and resieving at the lower size range to remove heavily etched lighter minerals and outer portions of grains which had received an alpha dose. Sample purity after preparation was tested using infrared stimulated luminescence; no significant contamination was observed in any sample.

With regard to palaeodose (D_e) measurement, in order to mitigate against erroneous inclusion of D_e data from post-depositional disturbance or partial bleaching, a variety of measurement levels and statistical analyses were adopted using the decision process shown in Supplementary Fig. 4. D_e values for all samples were initially measured at the single aliquot level using 9.6 mm diameter discs coated with a monolayer of grains and Risø automated luminescence readers with stimulation provided either by a filtered 150W halogen lamp or blue diodes. OSL signal was detected through a Hoya U340 filter with measurements carried out for 80s at 125°C. D_e measurement used the single aliquot regeneration (SAR) protocol[34] with four regeneration points and a recycling dose (Supplementary Fig. 5). For each single aliquot OSL measurement, the first 1.6 sec were used as signal and the final 12 sec averaged and subtracted as background (Supplementary Fig. 5). Preheat temperatures for the SAR protocol were either 180°C or 220°C for 10s as determined using a dose recovery preheat plateau test[35]. A cutheat of 160°C was used prior to measurement of all OSL responses to the test dose. All samples exhibited low thermal transfer, good recycling, and OSL decay curves indicating that the signal was dominated by the fast component and rapidly bleachable (Supplementary Fig. 5).

Spot checks with single grain measurements showed that only 1–7% of grains contributed 90% of the OSL signal[36], thus each single aliquot averaged the OSL signal of between approximately 15 and 550 grains. Single aliquot measurements were therefore considered relatively effective in isolating samples which might have multiple D_e components. As a result, multiple D_e replicates of each sample were measured to give an indication of D_e reproducibility (Supplementary Fig. 6). Where overdispersion (OD) for samples was less than 25% and the D_e distribution was unimodal and unskewed (Group A of Supplementary Fig. 4), ages were calculated using a D_e value derived from a weighted mean (by inverse variance). Samples Shfd02040, Shfd02041, Shfd02042, Shfd02047, Shfd02066 and Shfd02067 were previously reported with ages based on weighted mean D_e values once outliers (values outside 2 sigma of the mean) had been excluded[6]. For consistency with the new data these were re-analyzed including previously excluded D_e data. As a result, whilst four ages remain unchanged because there were no outliers in the dataset, the reported age for Shfd02047 of 12.9 ± 0.8 kyr has been revised to 12.7 ± 0.8 kyr and the age for Shfd02041 revised from 10.7 ± 0.6 kyr to 11.5 ± 0.7 kyr.

Whilst the OD values for samples Shfd06117 and Shfd08147 (Group B of Supplementary Fig. 4) were less than 25%, the D_e distributions for both samples were more complex than would have been expected from well-bleached aeolian sediments. Both samples therefore underwent finite

mixture modelling[37]. Finite mixture modelling rather than the minimum age modelling[38] was undertaken as a precaution against the possibility that sediment which was inherently too young had been incorporated through post-depositional disturbance. The finite mixture model was run a number of times with a sigma b value of 0.1, increasing the number of components until the Bayesian Information Criterion was minimized[39]. Results of this analysis found three components in each sample. Shfd08147 was sampled from foresets just beneath glaciotectonic structures where some post-depositional disturbance had clearly occurred, which could have introduced younger sediment. In light of this, the second lowest D_e component extracted by finite mixture modelling, representing 50% of the data, was selected for use in age calculation. The slightly multi-modal/skewed D_e distribution for sample Shfd06117 was more difficult to interpret. If the weighted mean D_e, which represented the bulk of the D_e data, was used this returned a sample age of 17.5 ± 1.1 kyr indicating a significant temporal hiatus between preserved aeolian sediments and the overlying flood deposits at Section MB05-01 (Supplementary Fig. 3B). However, as the sample was taken from undeformed and well-preserved dune foresets, post-depositional disturbance is discounted and the skewing of the D_e distribution could be interpreted as indicating inclusion of some partially bleached sediment within the sample. If the smallest finite mixture model extracted D_e component, which represents 17% of the total data, is used for age calculation purposes an age estimate of 13.4 ± 0.9 kyr is returned. Whilst we cannot discount an age of 17.5 ± 1.1 kyr, we are of the opinion that this younger age most likely reflects the final burial age of the sediment and avoids age over-estimation due to any partially bleached sediment. If, however, the older age is accepted the average pre-flood age of sediment (weighted mean by inverse variance) would be 13.3 ± 0.5 kyr instead of the reported 13.0 ± 0.2 kyr.

For samples where OD exceeded 25% (Shfd06118, Shfd06119, Shfd06120) further analysis at the single grain level was undertaken. Single grain measurements were performed on a TL-DA-15 Risø single grain reader with individual grains stimulated with a Nd:YVO_4 laser[40]. Single grain measurements followed the same SAR protocol as above, but as the OSL signal decays more quickly, the first 0.06 sec and final 0.2 sec were used for the signal and background calculations (Supplementary Fig. 5). Whilst single grain results for Shfd06119 showed a larger OD than the single aliquot data, there was no change in mean D_e when compared to the single aliquot data. Additionally, as no skewing or evidence of multiple D_e populations were apparent in the single grain data, a weighted mean D_e based on single aliquot results was used for age calculation. For samples Shfd06118 and Shfd06120 single grain analysis yielded a change in mean D_e when compared to the single aliquot data, with the D_e distributions displaying multi-dose components and skewing (Group C of Supplementary Fig. 4). As a result, for these samples the single grain D_e values were analysed using finite mixture modelling[37] using a sigma b value of 0.15. From this three components were extracted and the smallest D_e component which represented more than 10% of the data was selected for age calculation purposes[39].

Dose rates were determined from *in situ* field measurements made with an EG&G Micronomad field gamma-spectrometer. Where this was not possible due to logistical reasons analysis was undertaken using inductively coupled mass spectroscopy (ICP-MS) at SGS Laboratories, Canada. Conversions to annual dose rates followed Adamiec and Aitken[41] for alpha and gamma and Marsh *et al.*[42] for beta, with dose rates attenuated for sediment size and palaeomoisture contents. The latter were based on moisture content at time of sampling with an absolute error of 5% incorporated to allow for past changes. Cosmic dose rates were determined following Prescott and Hutton[43].

Supplementary Table 1 presents the OSL data results for the samples. Ages are quoted from year of sampling with 1-sigma uncertainties based on the propagation, in quadrature, of errors associated with D_e measurement, beta source calibration[44], palaeowater content, beta and gamma dose attenuation due to grainsize and uncertainties in published dose rate conversion co-efficients and algorithm for calculating cosmic dose.

Most of the aeolian sediment dated should have been well bleached prior to burial, as shown in Bateman and Murton[6], and the fluvial sand dated is likely to have been reworked from the underlying well-bleached aeolian material. Whilst the D_e scatter shown in Supplementary Fig. 6 indicates more D_e scatter within some samples than would normally be expected for well-bleached undisturbed sediments, we believe the measurement and statistical procedures adopted minimize the impact and that the ages reflect the true burial age of the sediment. The OSL chronology reported in ref. 6 was independently validated with three radiocarbon dates, obtained from *in situ* wood within an aeolian sand sheet, providing ages in agreement with 3 stratigraphically associated OSL ages on aeolian quartz sand.

Supplementary Tables

Supplementary Table 1. OSL sample data and ages with 1 sigma uncertainties from the Richards Island region.

Site	Lab. Code	Grain Size (μm)	Water content (%)	K (%) [c]	U (ppm) [c]	Th (ppm) [c]	Total dose rate (μGy a^{-1})	D_e (Gy) [d]	Age (kyr)
CP3.11[a]	Shfd02066	90-125	4.0 ± 5	1.03	1.30	3.77	1.72 ± 0.09	16.1 ± 1.0	9.3 ± 0.7
HW3.1b[a,b]	Shfd02041	90-125	4.3 ± 5	1.21	1.38	4.10	1.92 ± 0.10	22.1 ± 0.7	11.5 ± 0.7
MB05-01	Shfd06118	125-180	4.2 ± 5	1.10	1.48	4.00	1.78 ± 0.09	20.9 ± 1.4[f,g]	11.8 ± 1.0
MB05-02	Shfd06119	180-250	2.9 ± 5	1.13	1.26	4.00	1.67 ± 0.08	19.9 ± 1.4	11.9 ± 1.0
MB05-01	Shfd06117	180-212	2.0 ± 5	0.85	1.36	3.56	1.49 ± 0.07	19.9 ± 1.0[g]	13.4 ± 0.9
MB05-02	Shfd06120	125-180	4.3 ± 5	1.13	1.26	3.99	1.78 ± 0.09	22.9 ± 1.5[f,g]	12.9 ± 1.1
SB05-01	Shfd06066	125-180	2.8 ± 5	1.05	1.15	3.64	1.70 ± 0.09	22.0 ± 0.8	12.9 ± 0.8
Had 3.1b[a]	Shfd02042	90-125	5.0 ± 5	1.17	1.51	4.61	1.93 ± 0.10	24.6 ± 0.9	12.8 ± 0.8
CP3.11[a]	Shfd02067	90-125	3.3 ± 5	1.05	1.35	3.27	1.74 ± 0.09	22.8 ± 1.1	13.2 ± 0.9
Had 3.1b[a,b]	Shfd02047	90-125	4.8 ± 5	1.17	1.72	4.62	1.92 ± 0.10	24.3 ± 0.9	12.7 ± 0.8
SB08-12	Shfd08147	125-180	4.3 ± 5	1.08	1.55	4.4	1.84 ± 0.09[e]	23.3 ± 1.2[g]	12.7 ± 0.9
Had 3.1a[a]	Shfd02040	90-125	6.0 ± 5	1.26	1.46	4.37	1.97 ± 0.10	1.3 ± 0.1	0.7 ± 0.1
MB05-02	Shfd06121	125-180	5.0 ± 5	1.03	1.29	3.40	1.68 ± 0.08	0.4 ± 0.01	0.2 ± 0.01

[a] samples reported in Ref. 6. [b] age data revised using methodology outline in text. [c] Uncertainties applied were 5% for K and 10% for U and Th. [d] D_e given with associated standard error. [e] Dose rate based on analysis of sediment by ICP-MS rather than by *in situ* gamma-spectroscopy. [f] Measured at the single grain level. [g] D_e derived by finite mixture modelling[38] which found three components for Shfd06117, Shfd06118, Shfd06120 and Shfd08147.

Supplementary Table 2. Radiocarbon ages from the Fort McMurray region.

^{14}C Date (yr BP; 1σ range)	Lab Number	Calibrated age (cal. yr BP; 2σ range)*	Material Dated	Location	Source of Information
9,910 ± 190	GSC-4302	10766-12059	Wood	Athabasca Delta (58°15' N, 111°25' W)	Smith (1994)[45]
9,710 ± 130	AECV-1183C	10654-11403	Wood	Athabasca Delta (58°15' N, 111°25' W)	Smith (1994)[45]
9,850 ± 80	Wat-2661	11124-11507	Wood	Peace Delta (58°53'N, 113°02'W)	Smith (1994)[45]
10,600 ± 120	GSC-4821	12230-12840	Gyttja	Nipawin Bay (56°24'28" N, 108°33'00"W)	Anderson and Lewis (1992)[46]
10,000 ± 35	UCIAMS34698	11282-11624	Birch bracts, alder nutlet, willow bud, stem fragment	Nipawin Bay (56°24'28" N, 108°33'00")	Teller, 2007, unpublished
11,100 ± 150	GSC-4807	12836-13252	Plant detritus	Long Lake (56°51'40"N, 108°59'20"W)	Anderson and Lewis (1992)[5]
10,310 ± 290	GX-5031-II†	11245-12816	Shells†	Syncrude Mine (56°59'50"N, 111°29'49"W)	Syncrude (1977), unpublished; Smith & Fisher (1993)[18]
10,015 ± 320	GX-5036-I	10687-12678	Wood Fragments	Syncrude Mine (56°59'50"N, 111°29'49"W)	Syncrude (1977), unpublished; Smith & Fisher (1993)[18]
11,405 ± 245	GX-5036-II	12888-13740	Shells	Syncrude Mine (56°59'50"N, 111°29'49"W)	Syncrude (1977), unpublished
13,075 ± 340	GX-5030-II	14277-16421	Shells	Syncrude Mine (56°59'50"N, 111°29'49"W)	Syncrude (1977), unpublished
10,040 ± 60	Unknown	11272-11821	Twigs	Fort Hill, Syncrude Aurora Lease Area (57°20'49"N, 111°29'57"W)	Syncrude (2005), unpublished
10,400 ± 180	Unknown	11618-12810	Wood	Fort Hill, Syncrude Aurora Lease Area (57°20'49"N, 111°29'57"W)	Syncrude (2005), unpublished
11,280 ± 275	GX8910	12794-13738	Bulk sediment with bitumen removed	Eaglenest Lake	Vance (1986)[47]
11,300 ± 110	GSC-2038	12958-13362	Clayey gyttja	Mariana Lake	Hutton & MacDonald (1994)[48]
10,040 ± 50	Beta-200072	11312-11771	Wood	Cabin Lake	Fisher *et al.* (2009)[49]
10,030 ± 75	ETH-30177	11259-11825	Wood	Hook Lake	Fisher *et al.* (2009)[49]
10,270 ± 50	Beta-194058	11816-12239	Wood	Deep Hole Lake	Fisher *et al.* (2009)[49]
10,310 ± 75	ETH-32165	11813-12396	Wood	Mariana Lake	Fisher *et al.* (2009)[49]
10,460 ± 65	ETH-30586	12124-12669	Wood	Don's Lake	Fisher *et al.* (2009)[49]

* Converted to calibrated years based on Reimer *et al.* (2004)[50], using version 5.0.2 http://calib.quab.ac.uk/calib (2009). † Published by Smith and Fisher (1993)[18] as GX-5301-II, with dated material incorrectly noted as wood.

Supplementary Discussion

Gravelly deposits

Gravelly deposits above an erosion surface are widespread within a few metres of the ground surface of NE Richards Island (Fig. 2). The deposits comprise a pebble to boulder lag, gravel or pebbly sand—examined in this study and in previous studies[5,32,51–56]—at measured elevations ranging from 1 m.a.s.l. to 30 m.a.s.l. (Fig. 2). We have observed them as either one or two distinct stratigraphic units, interbedded in sequences of aeolian or fluvial sand[6,51], the higher unit sometimes overlain by peat. At Mason Bay section 05-02, a lower bed of gravel contains boulders of maximum dimension 0.37 m and overlies an erosion surface with a channelled base (Supplementary Fig. 3A). The gravel is fluvial in origin because it overlies a channelled erosion surface and is interbedded with aeolian sand[51]. The gravel was probably in part reworked from Toker Point till[51–52,54–55] because it contains erratics derived from the Canadian Shield that are similar to those in nearby till, and it also occurs where the till is absent. After fluvial erosion and deposition ceased, renewed wind action later buried some of the gravelly deposits beneath aeolian sand. Elsewhere, peat buried them.

Gravelly deposits are also common offshore on the Akpak Plateau to the north of Richards Island and on the Kringalik Plateau to the northwest of it (Supplementary Fig. 1). The deposits—recorded in numerous borehole logs and seafloor grab samples during hydrocarbon exploration and search for granular materials in the Beaufort Sea[33,57–64]—crop out at the seabed or are buried to depths of ~15 m below it in water between ~1 m and 15 m deep. The deposits include pebble to cobble-size material, occasionally with boulders as large as 0.5 m[65]. They range in occurrence from a lag, through pebbly sand to gravel, and their thickness generally varies between ~0.1 m and 1.0 m. They often occur at the base of unit B[66–67], directly above the regional unconformity that we correlate onshore to Richards Island (Supplementary Fig. 2; see below). The gravelly deposits have been interpreted as lag deposits formed during Holocene marine transgression[33,66–68] and, in places, as older fluvial or fluvial deltaic deposits, but lacking evidence for source river channels[65,69]. We suggest that some of the gravel was deposited by outburst flooding, as on northern Richards Island, and that in regions that are now offshore some of the gravel may also record reworking above wave base during the Holocene marine transgression.

Late Quaternary history and land-sea correlations

The similar pre-Holocene history of the eastern shelf and northeastern Richards Island facilitates land-sea correlations (Supplementary Fig. 2)[5,31]. During the last Glacial period much of the eastern Beaufort Shelf was emergent and subject to permafrost development, fluvial and then aeolian[6,70] activity, prior to Laurentide glaciation during the Toker Point Stade. Glaciation of Richards Island during this stade is thought to have occurred sometime between ~22 kyr ago and 16 kyr ago[56], when Laurentide ice deposited till across this region[30]. Associated glaciofluvial features such as eskers and abandoned valley systems in places resemble supraglacial systems on modern glaciers, and basal ice from this ice sheet is still preserved beneath supraglacial melt-out till[12]. Deglaciation had commenced by 16 kyr ago (see summary in ref. 56). As the active ice margin retreated south towards and beyond the Sitidgi Stade limit, aeolian dune building, sand-sheet aggradation and sand-wedge formation[56] recommenced in the northeastern Richards Island

region. This second period of aeolian deposition began at ~16 kyr ago[6,56] and abruptly ended shortly after 13.0 ± 0.2 kyr ago (Table 1) as a result of the fluvial erosion discussed in this paper. Holocene marine transgression later submerged part of the shelf.

A regional unconformity offshore truncates sand of unit C that correlates onshore with the aeolian Kittigazuit Formation and the underlying fluvial Kidluit Formation[31]. The unconformity offshore also truncates patches of diamicton that correlate onshore with Toker Point till[31]. The unconformity developed by fluvial erosion during the last Glacial-Interglacial transition and, offshore, was later submerged, trimmed and—in many places—buried during the Holocene marine transgression. Blasco *et al.*[7] attributed the offshore unconformity to erosion and reworking of the top of unit C by the transgression. A compound origin, however, is likely[33,71] because (a) prior to this transgression, fluvial activity eroded the top of unit C/Kittigazuit Fm and incised channels and valleys into the shelf (subaerial erosion phase discussed by Lewis[33,71]); and (b) the overlying gravelly deposits onshore have never experienced marine transgression.

An unconformity is also present in the Mackenzie Trough (Supplementary Fig. 1), along the top of sediments attributed to delta progradation during the Sitidgi Stade[9]. The unconformity has been interpreted as a flooding surface resulting from ice-margin retreat and early Holocene sea-level rise[9]. A revised interpretation, proposed here, is that it correlates with the erosion surface on northern Richards Island and offshore on the eastern shelf. We suggest that the surface initially developed by fluvial erosion and was later buried by marine sediments as sea level rose.

The interpretations given in this paper provide a basis to assess and model the palaeooceanographic response of the Arctic Ocean to deglacial flooding through the Mackenzie River, as well as to re-interpret the palaeogeography, age and origin of sediments found in the lower Mackenzie Valley/Delta and southern Beaufort Sea.

Supplementary Notes

References

30. Rampton, V. N. *Quaternary Geology of the Tuktoyaktuk Coastlands, Northwest Territories.* (Geological Survey of Canada, Memoir 423, 1988).

31. Dallimore, S. R. in *Geological, geotechnical and geophysical studies along an onshore-offshore transect of the Beaufort Shelf.* (ed Dallimore, S. R.) 250–255 (Geological Survey of Canada, Open File 2408, 1991).

32. Terrain Analysis & Mapping Services Limited. *Potential Granular Resources and their Geological Constraints, Northern Richards Island.* (Report for Department of Indian Northern Affairs, 1993).

33. Lewis, J. F. in *Proceedings of the Beaufort Sea Granular Resources Workshop, February 13 and 14, 1992.* (ed MacLeod, N. R.) 51–75 (EBA Engineering Consultants Ltd, Calgary, 1993).

34. Murray, A. S. & Wintle A. G. Luminescence dating of quartz using an improved single-aliquot regenerative-dose protocol. *Radiation Measurements* **32,** 57–73 (2000).

35. Murray, A. S. & Wintle A. G. The single-aliquot regenerative-dose protocol: potential for improvements in reliability. *Radiation Measurements* **37,** 377–381 (2003).

36. Duller, G. A. T. Single-grain optical dating of Quaternary sediments: why aliquot size. *Boreas* **37**, 589–612 (2008).

37. Roberts, R. G., Galbraith, R. F., Yoshidaa, H., Laslett, G. M. & Olley, J. M. Distinguishing dose populations in sediment mixtures: a test of single-grain optical dating procedures using mixtures of laboratory-dosed quartz. *Radiation Measurements* **32,** 459–465 (2000).

38. Olley, J. M., Pietsch, T. & Roberts, R. G. Optical dating of Holocene sediments from a variety of geomorphic settings using single grains of quartz. *Geomorphology* **60,** 337–358 (2004).

39. Bateman, M. D., Murton, J. B. & Boulter, C. The source of De variability in periglacial sand wedges: depositional processes versus measurement issues. *Quaternary Geochronology* (in press).

40. Duller, G. A. T, Bøtter-Jensen, L., Murray, A. S. & Truscott, A. J. Single grain luminescence (SGLL) measurements using a novel automated reader. *Nuclear instruments and methods in physics research Section B: beam interactions with materials and atoms* **155,** 506–514 (1999).

41. Adamiec, G. & Aitken, M. J. Dose-rate conversion factors: update. *Ancient TL* **16**, 37–50. (1998)

42. Marsh, R. E., Prestwich, W. V., Rink, W. J. & Brennan, B. J. Monte Carlo determinations of the beta dose rate to tooth enamel. *Radiation Measurements* **35,** 609–616 (2002).

43. Prescott, J. R. & Hutton, J. T. Cosmic ray contributions to dose rates for luminescence and ESR dating: large depths and long-term variations. *Radiation Measurements* **23,** 497–500 (1994).

44. Armitage, S. J. & Bailey, R. M. The measured dependence of laboratory beta dose rates on sample grain size. *Radiation Measurements* **39**, 123–127 (2005).

45. Smith, D. G. Glacial Lake McConnell: paleogeography, age, duration, and associated river deltas, Mackenzie River basin, western Canada. *Quat. Sci. Rev.* **13**, 829–843 (1994).

46. Anderson, T. W. & Lewis, C. F. M. in *Current Research, Part B.* 7–11 (Geological Survey of Canada, Paper 92-1B, 1992).

47. Vance, R. E. Pollen stratigraphy of Eaglenest Lake, northeastern Alberta. *Can. J. Earth Sci.* **23**, 11–20 (1986).

48. Hutton, M. J. & MacDonald, G. M. Postglacial vegetation history of the Mariana Lake region, Alberta. *Can. J. Earth Sci.* **31**, 418–425 (1994).

49. Fisher, T. G., Waterson, N., Lowell, T. V. & Hajdas, I. Deglaciation ages and meltwater routing in the Fort McMurray region, northeastern Alberta and northwestern Saskatchewan, Canada. *Quat. Sci. Rev.* **28**, 1608–1624 (2009).

50. Reimer, P. J. *et al.* IntCal04 Atmospheric radiocarbon age calibration, 26–0 ka BP, *Radiocarbon* **46**, 1026–1058 (2004).

51. Murton, J. B., French, H. M. & Lamothe, M. Late Wisconsinan erosion and eolian deposition, Summer Island area, Pleistocene Mackenzie Delta, Northwest Territories: optical dating and implications for glacial chronology. *Can. J. Earth Sci.* **34,** 190–199 (1997).

52. Dallimore, S. R. & Vincent, J-S. in *Geological, geotechnical and geophysical studies along an onshore-offshore transect of the Beaufort Shelf.* (ed Dallimore, S. R.) 20–25 (Geological Survey of Canada, Open File 2408, 1991).

53. Murton, J. B. Ground-ice stratigraphy and formation at North Head, Tuktoyaktuk Coastlands, Western Arctic Canada: a product of glacier–permafrost interactions. *Permafrost Perigl. Process.* **16,** 31–50 (2005).

54. Hardy Associates (1978) Surficial Geology of the area around Illisarvik, Richards Island, Northwest Territories. (Geological Survey of Canada, Open File 941, 1983).

55. Fyles, J. G., Heginbottom, J. A. & Rampton, V. N. *Quaternary geology and geomorphology, Mackenzie Delta to Hudson Bay* (XXIV International Geological Congress, Guidebook Excursion A-30, 1972).

56. Murton, J. B., Frechen, M. & Maddy, D. Luminescence dating of Mid- to Late Wisconsinan aeolian sand as a constraint on the last advance of the Laurentide Ice Sheet across the Tuktoyaktuk Coastlands, western Arctic Canada. *Can. J. Earth Sci.* **44,** 857–869 (2007).

57. EBA Engineering Consultants Ltd. *Beaufort Sea Database Volume 3. Borehole Logs for the Beaufort Sea, Dome Petroleum Ltd 1974–1980.* (Report for Department of Indian and Northern Affairs, 1988).

58. EBA Engineering Consultants Ltd. *Beaufort Sea Database Volume 4. Borehole Logs for the Beaufort Sea, Esso Resources Canada Ltd 1974.* (Report for Department of Indian and Northern Affairs, 1988).

59. EBA Engineering Consultants Ltd. *Beaufort Sea Database Volume 5. Borehole Logs for the Beaufort Sea, Dome Petroleum Ltd 1981–1982.* (Report for Department of Indian and Northern Affairs, 1988).

60. EBA Engineering Consultants Ltd. *Beaufort Sea Database Volume 6. Borehole Logs for the Beaufort Sea, Esso Resources Canada Ltd 1975.* (Report for Department of Indian and Northern Affairs, 1988).

61. EBA Engineering Consultants Ltd. *1988 Offshore Geotechnical Site Investigation. Proposed North Point Pipeline Route, Beaufort Sea.* (Report for Gulf Canada Resources Ltd, 1988).

62. EBA Engineering Consultants Ltd. *Beaufort Sea Database 1989. Surficial Sediment and Borehole Log Data Volume I, Surficial Sediment and Borehole Logs for the Isserk and Erksak regions of the Beaufort Sea.* (Report for Department of Indian and Northern Affairs, 1989).

63. EBA Engineering Consultants Ltd. *Beaufort Sea Database 1989. Surficial Sediment and Borehole Log Data Volume II, Surficial Sediment and Borehole Logs for the Beaufort Sea.* (Report for Department of Indian and Northern Affairs, 1989).

64. EBA Engineering Consultants Ltd. *Beaufort Sea Database 1989. Surficial Sediment and Borehole Log Data Volume III, Surficial Sediment and Borehole Logs for the Beaufort Sea.* (Report for Department of Indian and Northern Affairs, 1989).

65. EBA Engineering Consultants Ltd. *Synthesis and Interpretation of Bathymetric, Geophysical and Geotechnical Data from Issigak Borrow Block.* (Report for Indian and Northern Affairs Canada, 1987).

66. Blasco, S. M. in *Proceedings of the Beaufort Sea Granular Resources Workshop, February 13 and 14, 1992.* (ed MacLeod, N. R.) 160–175 (EBA Engineering Consultants Ltd, Calgary, 1993).

67. EBA Engineering Consultants Ltd. *Geotechnical/Geological Investigation of Selected Granular Resource Prospects: Beaufort Sea.* (Report for Indian and Northern Affairs Canada, 1995).

68. Hill, P. R. & Solomon, S. Geomorphologic and sedimentary evolution of a transgressive thermokarst coast, Mackenzie Delta region, Canadian Beaufort Sea. *J. Coastal Res.* **15**, 1011–1029 (1999).

69. MacLeod, N. R. in *Proceedings of the Beaufort Sea Granular Resources Workshop, February 13 and 14, 1992.* (ed MacLeod, N. R.) 30–50 (EBA Engineering Consultants Ltd, Calgary, 1993).

70. Dallimore, S. R., Wolfe, S. A., Matthews, J. V. Jr. & Vincent, J-S. Mid-Wisconsinan eolian deposits of the Kittigazuit Formation, Tuktoyaktuk Coastlands, Northwest Territories, Canada. *Can. J. Earth Sci.* **34,** 1421–1441 (1997).

71. Lewis, J. F. *Review of Granular Resource Potential: South-central Beaufort Sea with Identification of Field Investigation Targets.* (Report for Department of Indian and Northern Affairs, 1994).